

LEVEL

NUSC Technical Report 6339

NUSC Technical Report 6339

AD A094266



DTIC
ELECTE
JAN 29 1981
S
D
13
S

Performance of the Optimum and Several Suboptimum Receivers for Threshold Detection of Known Signals in Additive, White, Non-Gaussian Noise

Raymond F. Ingram
Robert Houle
Submarine Electromagnetic Systems Department

24 November 1980

NUSC

Naval Underwater Systems Center
Newport, Rhode Island • New London, Connecticut

Approved for public release; distribution unlimited.

DDC FILE COPY

81 1 29 040

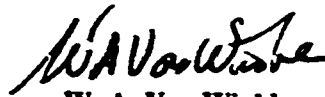
Preface

This research was conducted under NUSC's IR/IED Project No. A51200, "Nonlinear Noise Processing," Principal Investigator, R. F. Ingram (Code 341), Program Element, 61152N, Navy Subproject and Task No. ZR 000 01 01, Program Manager, J. H. Probus (NAVMAT 08T1).

The Technical Reviewer for this report was A. H. Nuttall (Code 3302).

The authors would like to thank R. J. Aiksnoras (Code 341) for his assistance in measuring ELF noise distributions and the fitting of them to Middleton's Class B Noise Model.

Reviewed and Approved: 24 November 1980



W. A. Von Winkle
Assistant Technical Director for Technology

The authors of this report are located at the
New London Laboratory, Naval Underwater Systems Center
New London, Connecticut 06320.

TABLE OF CONTENTS

	Page
LIST OF ILLUSTRATIONS	iii
INTRODUCTION	1
OPTIMUM RECEIVER STRUCTURE	1
PERFORMANCE MEASURE	3
CANONICAL NOISE MODEL	5
COMPARISON OF NONLINEAR DEVICES IN CLASS B NOISE ENVIRONMENT	7
ELF RECEIVER PERFORMANCE	8
CONCLUSIONS	9
REFERENCES	25
APPENDIX A--DERIVATION OF THE IMPROVEMENT FACTORS FOR SEVERAL NONLINEARITIES	A-1
APPENDIX B--NUMERICAL COMPUTATION OF THE HYPERGEOMETRIC AND GAMMA FUNCTIONS	B-1

Accession For	
NTIS GRA&I	<input checked="" type="checkbox"/>
DTIC TAB	<input type="checkbox"/>
Unannounced	<input type="checkbox"/>
Justification	<input type="checkbox"/>
By _____	
Distribution/ _____	
Availability Codes _____	
Dist	Avail and/or Special
A	

LIST OF ILLUSTRATIONS

Figure		Page
1	Block Diagram of Optimum Receiver	10
2	Typical Noise Densities and Resulting Transfer Functions	10
3	Simple Suboptimal Nonlinearities	11
4	Middleton's Class B Noise Probability Density Function, Where $A_\alpha = 1.0$ and Various α	11
5	Middleton's Class B Noise Probability Density Function, Where $\alpha = 1.0$ and Various A_α	12
6	Variation of I_{opt} and I_{opt}/σ^2 With Dynamic Range	13
7	Improvement Factor for Optimum Nonlinearity, Where $A_\alpha = 0.01$	14
8	Improvement Factor for Optimum Nonlinearity, Where $A_\alpha = 0.1$	15
9	Improvement Factor for Optimum Nonlinearity, Where $A_\alpha = 1.0$	16
10	Improvement Factor for Optimum Nonlinearity, Where $A_\alpha = 1.5$	17
11	Clipper Performance Relative to Optimum Performance, Where $A_\alpha = 0.01$	18
12	Clipper Performance Relative to Optimum Performance, Where $A_\alpha = 1.0$	19
13	Clipper Performance Relative to Optimum Performance, Where $A_\alpha = 1.5$	20
14	Hole Puncher Performance Relative to Optimum Receiver	21
15	APD of High Level ELF Noise, Where $A_\alpha = 1.5$ and $\alpha = 1.4$	22
16	APD of High Level ELF Noise, Where $A_\alpha = 1.0$ and $\alpha = 1.2$	23
17	APD of High Level ELF Noise, Where $A_\alpha = 1.0$ and $\alpha = 1.2 - 1.4$	24
A-1	Optimum Receiver Structure for Threshold Detection	A-1
B-1	Graphical Representation of the Quadratic Function $\frac{(n+1)! z^{n+1}}{(a)_n (a+1-b)_n} (t_{n+1} - t_n)$	B-3
B-2	Flow Diagram for Evaluating the Hypergeometric Function	B-5
B-3	Flow Diagram for Evaluating the Gamma Function	B-6

PERFORMANCE OF THE OPTIMUM AND SEVERAL SUBOPTIMUM
RECEIVERS FOR THRESHOLD DETECTION OF KNOWN SIGNALS
IN ADDITIVE, WHITE, NON-GAUSSIAN NOISE

INTRODUCTION

The additive noise encountered at a receiver input is often non-Gaussian. If the non-Gaussian nature of the noise is not taken into account in the design of the receiver, significant performance degradation of the receiver can be expected. The purpose of this technical report is to describe the performance that can be expected from the optimum and several suboptimum receivers used for detecting known threshold signals in an additive, white (i.e., statistically independent noise samples), non-Gaussian noise environment.

The optimum receiver structure for detecting known threshold signals in additive, white, non-Gaussian noise is the same as that which should be used if the noise were Gaussian, except that a zero memory nonlinearity is placed between the receiver input and the Gaussian detector. The input-output characteristic of the nonlinearity is given by $-d/dx (\ln p_n(x))$, where $p_n(x)$ is the density function of the noise alone. The measure of performance improvement obtained by including the nonlinear device is given by the ratio of the signal to noise ratio (SNR) at the receiver output with the nonlinearity in the circuit to the SNR at the receiver output without the nonlinearity. The magnitude of this improvement is evaluated here using Middleton's Class B Noise Model. The performance of several more easily implemented suboptimum nonlinearities, i.e., clipper, hole puncher, and hard limiter, are also evaluated using Middleton's model; and typical performances relative to the optimum are presented. Finally, the amplitude probability distributions (APD's) of high level extremely low frequency (ELF) noise are given and compared with the APD's resulting from Middleton's model. From these APD's and the parametric results presented, the expected performance of the optimum and suboptimum nonlinearities is derived.

OPTIMUM RECEIVER STRUCTURE

The optimum receiver structure for the threshold detection of binary coherent signals in an additive, white-noise environment is well known.¹⁻³ The derivation of this structure is summarized here.

Consider a discrete time, memoryless communication channel in which one of two known signals, $\underline{S}_1 = [S_{11}, S_{12}, \dots, S_{1N}]'$ or $\underline{S}_2 = [S_{21}, S_{22}, \dots, S_{2N}]'$, is transmitted every T seconds by successively transmitting the signal components, S_{ji} , ($i = 1, 2, \dots, N$), every Δt seconds. Each digit, z_i , in the received sequence of digits \underline{z} , is the sum of one of two known signals and a white-noise component, n_i . The receiver, then, must decide between the two hypotheses, $H_1: \underline{z} = \underline{S}_1 + \underline{n}$ and $H_2: \underline{z} = \underline{S}_2 + \underline{n}$, in such a manner that some criterion is optimized. For example, one may wish to minimize the expected

risk (Bayes Test) if costs have been assigned to all joint outcomes of correctly or incorrectly choosing a particular hypothesis. Alternatively, lacking such a cost structure, one may minimize the probability of an incorrect choice (Ideal Observer Scheme).

Because the noise is white and the signal components are known completely, the conditional probability density function of the received vector, \underline{z} , can be expressed in terms of the density functions of the individual noise components, $p_n(\alpha_i)$; i.e.,

$$p_{\underline{z}}(\underline{z}/H_j) = p_{\underline{z}}(z_1, z_2, \dots, z_N/H_j) = \prod_{i=1}^N p_n(z_i - S_{ji}) \quad (j = 1, 2) .$$

The receiver decides between H_1 and H_2 by comparing $p_{\underline{z}}(\underline{z}/H_1)$ with $p_{\underline{z}}(\underline{z}/H_2)$ relative to some constant threshold, λ , determined by the a priori probabilities of H_1 and H_2 and the optimality criterion. This is to say that the receiver forms the following likelihood ratio as its test statistic:

$$A = \frac{p_{\underline{z}}(\underline{z}/H_1)}{p_{\underline{z}}(\underline{z}/H_2)} = \frac{\prod_{i=1}^N p_n(z_i - S_{1i})}{\prod_{i=1}^N p_n(z_i - S_{2i})} \begin{matrix} H_1 \\ > \\ H_2 \end{matrix} \lambda .$$

Since the logarithm function is monotonic, an equivalent test is

$$\ln A = \sum_{i=1}^N \ln p_n(z_i - S_{1i}) - \sum_{i=1}^N \ln p_n(z_i - S_{2i}) \begin{matrix} H_1 \\ > \\ H_2 \end{matrix} \ln \lambda .$$

Considering the case of threshold detection, let the signal components, S_{ji} ($j = 1, 2, i = 1, 2, \dots, N$), be sufficiently small so that each term in the above expression can be expanded in a first order Taylor series about z_i . The log likelihood ratio test then becomes

$$\ln A = \sum_{i=1}^N \left[\ln p_n(z_i) - S_{1i} \frac{d}{dz_i} \ln p_n(z_i) \right]$$

$$- \sum_{i=1}^N \left[\ln p_n(z_i) - S_{2i} \frac{d}{dz_i} \ln p_n(z_i) \right] \begin{matrix} H_1 \\ > \\ H_2 \end{matrix} \ln \lambda ,$$

or

$$\ln \Lambda = \sum_{i=1}^N S_{1i} \left(-\frac{d}{dz_i} \ln p_n(z_i) \right) - \sum_{i=1}^N S_{2i} \left(-\frac{d}{dz_i} \ln p_n(z_i) \right) \underset{H_2}{\overset{H_1}{>}} \ln \lambda. \quad (1)$$

Equation (1) implies the block diagram of figure 1 for the optimal receiver structure. Note that it is just a correlation receiver in which a zero memory function, $-d/dz_i (\ln p_n(z_i))$, operates on the received signal prior to the correlation. Note also that the receiver is canonical; i.e., its general form and decision logic is not based on any particular model of the noise environment. However, the receiver must "know" (or estimate) the noise density function in order to implement the $-d/dz_i (\ln p_n(z_i))$ operation in the block diagram. If the noise environment is changing slowly in time, the optimal receiver must be adaptive.

When the noise is Gaussian, the $-d/dz_i (\ln p_n(z_i))$ function is linear in z_i and, as such, may be incorporated as a gain factor (weight) within the signal component, S_{ji} , so that the optimum receiver structure is exactly that of a correlator:

$$\text{Gaussian noise} \implies -\frac{d}{dz_i} \ln p_n(z_i) = -\frac{d}{dz_i} \ln \left[\frac{1}{\sqrt{2\pi\sigma^2}} e^{-z_i^2/2\sigma^2} \right] = \frac{z_i}{\sigma^2}.$$

For a non-Gaussian noise density, however, the derivative of the log density function is not a linear function of the received waveforms. Thus, the optimum receiver structure is a correlator preceded by a zero memory circuit whose input-output characteristics depend only on the noise probability density function.

As an example, it has been proposed that naturally occurring electromagnetic noise below 100 MHz is Gaussian distributed with occasional large amplitude noise bursts, which occur often enough to affect the tails of the noise density. Several authors⁵⁻⁶ have suggested that the density function describing these tails follows an $e^{-a|z|^k}$ ($0 < k < 1$) law. The smaller the k , the more impulsive the noise (see figure 2a). For this noise density, the input-output characteristic of the optimal nonlinearity is shown in figure 2b. As the noise becomes more impulsive, the nonlinear device suppresses the larger noise excursions to a greater degree.

PERFORMANCE MEASURE

After the optimal receiver structure has been derived, a natural question to ask is how much performance improvement can be expected using this receiver compared with one in which the nonlinearity prior to the correlator is sub-optimal or absent? Usually the performance of a receiver is measured by the probability of error for a given signal energy. This requires that the probability density function of the test statistic be known or, alternatively,

that the probability of error can be bounded in some manner. Under the assumption of threshold-type signals, the correlator must sum many received symbols to increase the SNR for satisfactory performance. As was seen previously, the nonlinear device tends to suppress large amplitude variations; thus, each received digit is bounded. (From a practical point of view, the received symbols are always bounded owing to the finite responses of amplifiers, filters, etc., even when the receiver is linear.) The test statistic, therefore, is the sum of independent, finite variance random variables and, by the Central Limit Theorem, is asymptotically Gaussian distributed. Since the density function of a normal random variable is completely specified by its mean and variance, the SNR at the output of the correlator may be used to express the receiver performance. Hence, define the improvement factor, I , as the ratio of the SNR's at the output of the receivers with and without a nonlinear noise processor:

$$I = \frac{\text{SNR}_{\text{NL}}}{\text{SNR}_{\text{L}}} = \frac{\text{SNR at output of receiver with nonlinearity present}}{\text{SNR at output of receiver with nonlinearity removed}}$$

Assuming threshold binary equal-energy signals, the improvement factor for the optimal receiver is (see appendix A)

$$I_{\text{opt}} = \sigma^2 \int_{-\infty}^{\infty} \left[-\frac{d}{dz} \ln p_n(z) \right]^2 p_n(z) dz = \sigma^2 \int_{-\infty}^{\infty} \frac{\left[\frac{d}{dz} p_n(z) \right]^2}{p_n(z)} dz, \quad (2a)$$

where σ^2 is the variance of a received symbol (i.e., the power of the noise component). When the noise is Gaussian, the improvement factor equals one.

Although the optimal receiver structure is canonical in form, it may be difficult to implement. This leads one to investigate simpler, suboptimal nonlinear processors using the improvement factor to compare the performance of various processors. Appendix A derives the improvement factor for three common nonlinear devices: the hard limiter, the clipper, and the hole puncher. The results are listed here for convenience:

$$I_{\text{HL}} = 4\sigma^2 p_n^2(0) \quad (2b)$$

$$I_{\text{C}} = p^2 \sigma^2 / \left[2 \int_0^c z^2 p_n(z) dz + c^2(1-p) \right] \quad (2c)$$

$$I_{\text{HP}} = \sigma^2 \left[p - 2c p_n(c) \right]^2 / \left[2 \int_0^c z^2 p_n(z) dz \right], \quad (2d)$$

where

$$p = \int_{-c}^c p_n(z) dz = \text{Probability of being in linear range of nonlinearity}$$

c = Linear range of nonlinearity (see figure 3).

The input-output characteristics of the above devices are shown in figure 3. Note that the hard limiter is the optimum nonlinearity when the noise has a density function of the form $p_n(z) = Ae^{-|z|}$. Comparing figure 2b with figure 3, one sees that the clipper is optimal and that the hole puncher is near optimal when the noise is Gaussian with tails distributed as $e^{-|z|^k}$ for $k = 1$ and 0 , respectively. It should also be pointed out that although the noise power, σ^2 , appears in each of the above expressions, it does not affect the comparison of one nonlinear device with another, though it certainly is important when comparing a nonlinear receiver with a linear one.

CANONICAL NOISE MODEL

As is evident in the above discussion, the optimal receiver structure is highly dependent on the probability density function of the noise. Although various noise models have been proposed for particular environments, the only general model available to date is that suggested by Middleton.⁷⁻⁹ His model, the Class B Noise Model, which is analytically tractable and is in excellent agreement with measured data for a variety of cases, is canonical in nature. That is to say the noise density function, which is characterized by various parameters, does not change form.

Based on the bandwidth of the interference relative to the receiver bandwidth, Middleton defines two major classes of noise. Of interest here is the Class B Noise Model in which the interference is highly impulsive, resulting in a noise bandwidth much greater than the receiver's front end bandwidth. For this case, the model for the amplitude noise probability density is expressible as two distinct functions: one valid for $|z| \leq z_{OB}$ and the other for $|z| > z_{OB}$. The second function approaches zero much more rapidly than the first as $z \rightarrow \infty$. It was already pointed out that a nonlinear device operating on threshold signals in this type of noise environment will suppress large voltage excursions in the received waveform. Thus, the noise power at the output of the nonlinear device is primarily determined by the noise density function, $p_n(z)$, for $|z|$ less than z_c , i.e., the value at which significant suppression occurs. The more impulsive the noise environment, the more likely z_c is much smaller than z_{OB} . For this reason, only the first function in Middleton's model is used here. Thus,

$$p_n(z) = p_I(z) \cong \frac{1}{\pi} \sum_{m=0}^{\infty} \frac{(-1)^m A^\alpha}{m!} \Gamma\left(\frac{m\alpha + 1}{2}\right) \cdot {}_1F_1\left(\frac{m\alpha + 1}{2}; \frac{1}{2}, -z^2\right) \quad |z| \leq z_{OB}, \quad (3)$$

where

$$0 < \alpha < 2, A_\alpha > 0$$

$\Gamma(\cdot)$ = Gamma Function

${}_1F_1(a; b; x)$ = Confluent Hypergeometric Function.

Three values, A_α , α , and z_{OB} , define the noise model. One can normalize the probability density function defined by these three values to unit variance, for $|z| \leq z_{OB}$, by introducing a fourth parameter, Ω . This is done by changing the variable of integration from z to \hat{z} as follows:

$$\begin{aligned} \sigma^2(z_{OB}) &\triangleq \int_{-z_{OB}}^{z_{OB}} z^2 p_n(z) dz \\ \Rightarrow 1 &= \int_{-\hat{z}_{OB}}^{\hat{z}_{OB}} \hat{z}^2 p_n(\hat{z}) d\hat{z} \end{aligned} \quad (4)$$

where

$$\hat{z} = z \sqrt{\Omega} \quad \hat{z}_{OB} = z_{OB} \sqrt{\Omega}$$

$$\Omega = 1/\sigma^2(z_{OB})$$

$$p_n(\hat{z}) = \frac{1}{\pi \sqrt{\Omega}} \sum_{m=0}^{\infty} \frac{(-1)^m A_\alpha^m}{m!} \Gamma\left(\frac{m\alpha + 1}{2}\right) {}_1F_1\left(\frac{m\alpha + 1}{2}; \frac{1}{2}; -\frac{\hat{z}^2}{\Omega}\right) \quad (5)$$

Typical density functions normalized for unit power with $z_{OB} = 10^4$ are plotted on a log-log scale in figures 4 and 5. Note that for constant A_α (figure 4), the more impulsive densities, i.e., those whose tails approach zero more slowly, are characterized by smaller α values. In fact, one can see in figure 5 that the slope of the tails is determined by the α parameter. Although the role of A_α is not as readily apparent as that of α , it is related to the slope of the density function during the transition from the Gaussian portion of the distribution to the non-Gaussian tails and to the range over which the density function is Gaussian-like. The "bendover" point, z_{OB} , is that point beyond which equation (3) no longer adequately describes the true density.

COMPARISON OF NONLINEAR DEVICES IN CLASS B NOISE ENVIRONMENT

The improvement factor of a nonlinear receiver is a function of the total noise power, the shape of the noise density function that yields that power, and the input-output characteristics of the nonlinear device. Equation (4) indicates that the noise power depends on z_{0B} , the bendover point in Middleton's Class B Noise Model. Intuitively, the more z_{0B} exceeds the suppression range of a nonlinear device, the greater the improvement factor for that device. An example of this can be seen in figure 6. Note that the increase in the improvement factor is entirely due to the increase in the variance once z_{0B} exceeds a particular value.

Figures 7, 8, 9, and 10 show the improvement factor for the optimal nonlinear receiver versus \hat{z}_{0B} for various noise statistics. (These results were obtained using equations (2a) and (4) and normalizing as in equation (5).) For these calculations $p_n(z)$ for $z > z_{0B}$ was assumed to be zero. As A_α approaches zero (figure 7), the density function is Gaussian over a greater range of values and, therefore, the improvement factor depends strongly on the shape of the tails. If the tails are decaying rapidly (larger α), only modest improvements are to be expected. On the other hand, if the tails approach zero very slowly (small α), significant processing gains may be achieved using the optimum nonlinear receiver over a linear one. As A_α increases (figures 8, 9, and 10), the noise is Gaussian over a smaller range of values; and improvements will occur at smaller values of \hat{z}_{0B} . Here, also, the shape of the tails greatly affect the processing gain. In general, for a given \hat{z}_{0B} , the improvement factors increase as A_α increases and as α decreases.

One of the primary goals of this report is to rate the performance of simpler suboptimal nonlinear receivers. The improvement factor for the hard limiter, the clipper, and the hole puncher were evaluated under a variety of noise conditions using Middleton's model and equations (2b)-(2d). Typical results are shown in figures 11-14. The performance of the clipper and the hole puncher are functions of the "clip level," i.e., the percentage of time the input is in the nonlinear portion of the device's operating characteristics. The hard limiter is a special case of the clipper in which the clip level is set at 100 percent.

Figures 11, 12, and 13 present the ratio of the clipper improvement factor to optimum improvement factor versus clip percentage for various A_α and α . While the optimum clip level, i.e., the clip level that results in the best performance, depends on the noise parameters defining the density function, the performance of the clipper relative to the optimum nonlinearity is not a strong function of the percentage of time that the input is in the nonlinear portion of the transfer function. In fact, by setting the clip level to obtain 90 percent clipping, the clipper performance will remain within about 4.5 dB of the optimum over a large range of noise parameters. When figures 7-10 are used as an absolute measure, the optimal improvement factor is large for just those values of α for which the clippers' performance decreases. As the optimal performance drops in value due to an increasing α , the clipper's performance increases so that, relatively speaking, the clipper is always close to the optimal.

Even simpler than the clipper is the hard limiter, which approaches the performance of the clipper without the requirement of adaptive control of the clip level. The more impulsive the noise, the closer the hard limiter's performance approaches that of the optimum clipper.

The relative performance of the hole puncher (figure 14) is very sensitive to both the clip level and the parameters of the noise density; but, when adjusted properly, it essentially can achieve optimal performance. Thus, while the transfer characteristic is easily implemented, logic is required to estimate the noise parameters, and adaptive control is needed to maintain the proper clip level.

The four nonlinear devices discussed in the report form a hierarchy of receivers based on complexity and performance. Although each application determines the exact tradeoffs, there are many cases in which the simpler suboptimal devices are more cost effective than the optimal.

ELF RECEIVER PERFORMANCE

In this section the general results obtained in the previous sections are applied to the ELF range of electromagnetic communications. Several digital tape recordings of typical high level ELF noise from the Saipan area were analyzed to yield amplitude probability distributions. These measured distributions are compared with distributions computed from Middleton's Class B Noise Model, equation (5), and the parameters A_α , α , and \hat{z}_{OB} are determined. From these parameter values and figures 7, 8, and 9 the expected performance for the optimum and suboptimum nonlinearities can be determined.

Figures 15-17 are plots of the amplitude probability distributions of typical high level ELF noise from Saipan. The noise was bandpass filtered to 20-150 Hz and each distribution was measured over 400 s. The ordinate of these figures is the percentage of time that the magnitude of the noise exceeds the abscissa level; the reference level of the abscissa is the rms level of the noise. The individual squares on the plots are points from Middleton's model. From these plots it is clear that the amplitude probability distributions and density functions of actual ELF noise can be described accurately by the amplitude distributions and densities resulting from Middleton's model. For these high levels of ELF noise, the parameter values range over $A_\alpha = 1.0 - 1.5$, $\alpha = 1.2 - 1.4$, and \hat{z}_{OB} approaching 40 dB. An optimally designed nonlinear receiver could be expected to perform 10-20 dB better than a linear receiver for these parameter ranges; however, the actual performance will depend on the particular combination of parameter values. If a clipper were utilized and set to clip between 20-80 percent of the time, its performance would be within about 1 dB of the optimum nonlinearity.

The current Propagation Validation System (PVS) ELF receiver utilizes a clipper that adjusts itself so that the received signal and noise is clipped 40 percent of the time. This rather simple device, which does not necessitate any complex noise parameter estimation, provides performance that is

comparable to that provided with the optimum nonlinearity. A detailed analysis of the nonlinear noise processing, including the aspects leading to the design and measured performance utilized in the Navy's ELF receivers, is contained in references 1 and 10.

CONCLUSIONS

The optimum receiver for detecting known threshold signals in additive, white, non-Gaussian noise has been described and its performance is defined as a function of the noise amplitude probability density function. The optimum receiver's performance has been calculated and plotted versus various ranges of the parameters defining Middleton's Class B Noise Model. From these plots it is apparent that the optimum nonlinear receiver can yield very significant performance improvements relative to the receiver that is optimum in Gaussian noise. Implementation of the optimum nonlinearity, however, can be rather complex, requiring real-time estimation of the noise parameters.

The performances of several suboptimum nonlinearities were calculated and their performance relative to the optimum was plotted. A properly adjusted hole puncher yields performance within 1 dB of the optimum; however, its' relative performance is very sensitive to the percentage of time the input is suppressed. Proper adjustment requires estimating the noise parameters, as is also required for the optimum nonlinearity. The performances of the clipper depend on the noise parameter values and the percentage of clip, as does the hole puncher; however, it is less sensitive to these values than is the hole puncher. A simple clipper adjusted to clip 90 percent of the time yields performance within 4.5 dB of the optimum over a wide range of noise parameters; the relative performance improves as the noise becomes less impulsive. The hard limiter, requiring no adjustment, yields performance within 2 dB of the optimum clipper; the performance relative to the optimum clipper improves as the noise becomes more impulsive.

The instantaneous amplitude probability density function resulting from Middleton's model fits measured high level ELF noise quite closely with $A_{\alpha} = 1.0 - 1.5$, $\alpha = 1.2 - 1.4$, and $\hat{z}_{0B} \approx 40$ dB. For this range of parameters, a clipper adjusted to clip 40 percent of the time, as does the PVS ELF receiver, provides performance within 0.5 dB of the optimum.

Recommendations for future work include

1. Determine optimum receiver's performance sensitivity to inaccuracies in parameter estimation.
2. Extend results to determine performance of these threshold receivers for nonthreshold signals.
3. Compare predicted performance of the optimum receiver, as defined here, at very low frequency (VLF) with measured performance of existing VLF receivers.

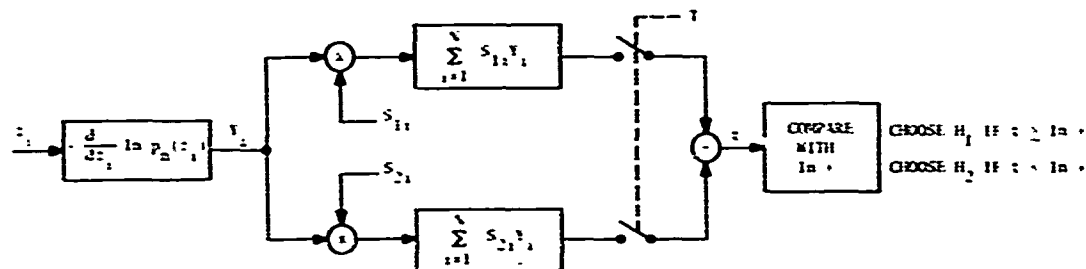


Figure 1. Block Diagram of Optimum Receiver

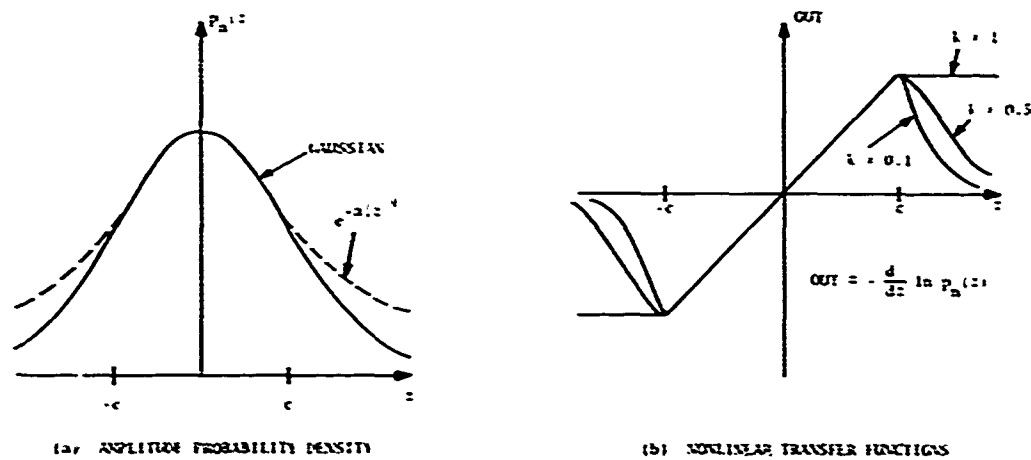


Figure 2. Typical Noise Densities and Resulting Transfer Functions

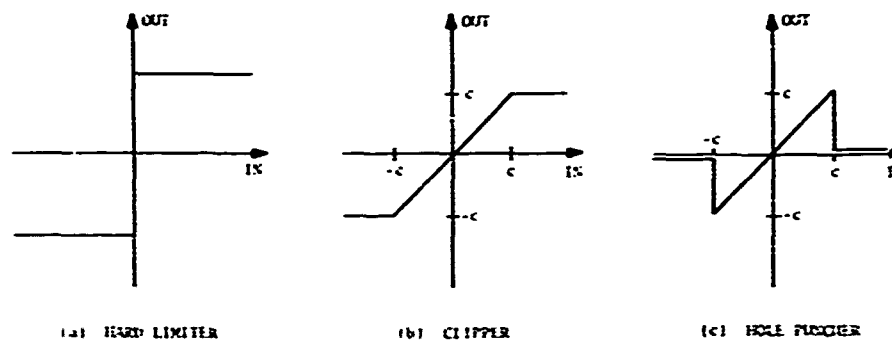


Figure 3. Simple Suboptimal Nonlinearities

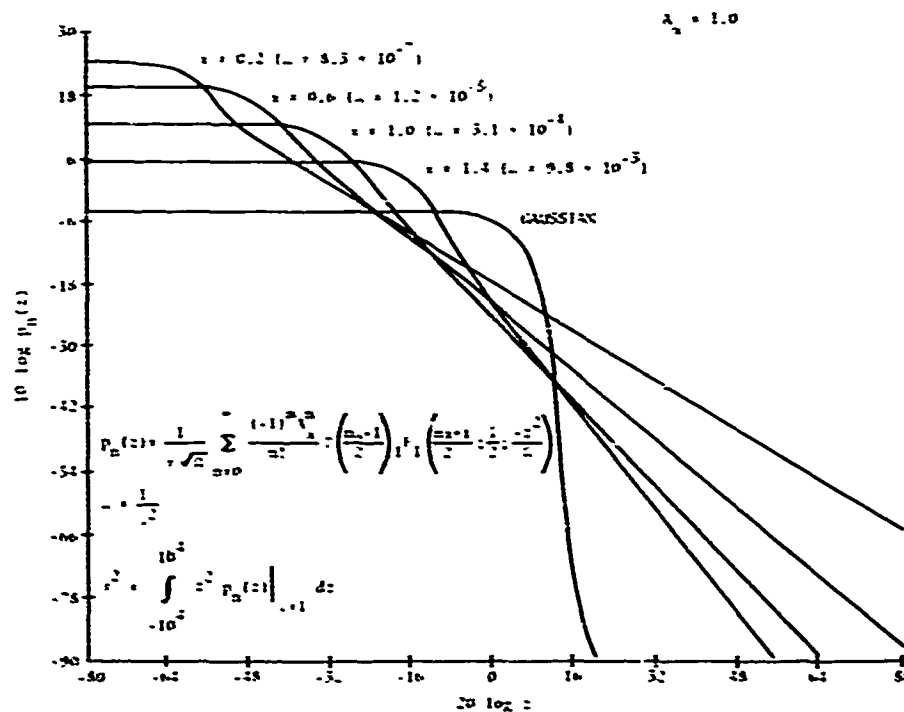


Figure 4. Middleton's Class B Noise Probability Density Function, Where $\lambda_{\alpha} = 1.0$ and Various α

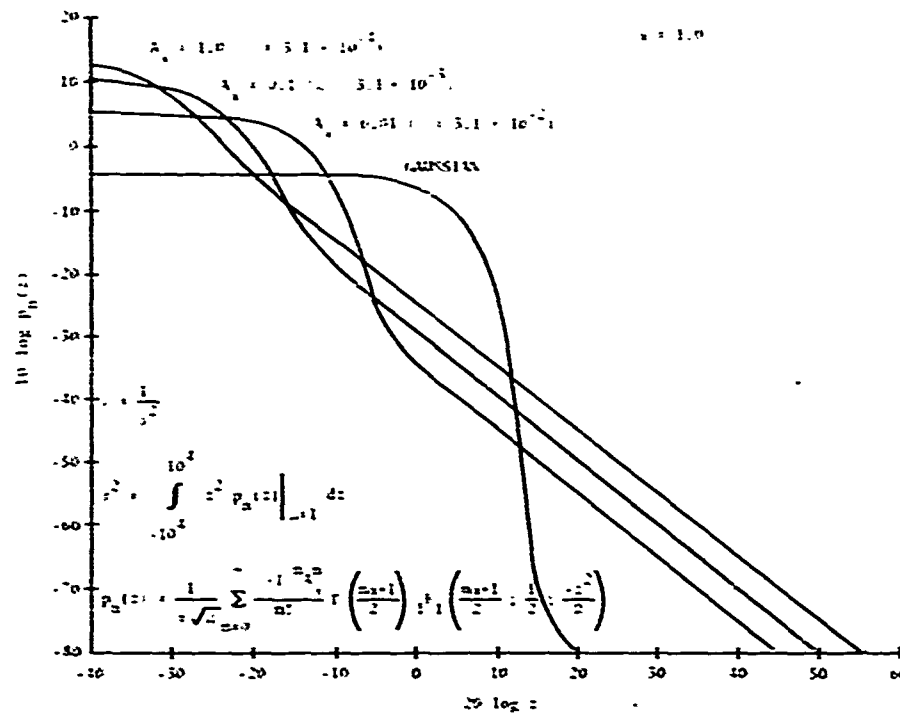


Figure 5. Middleton's Class B Noise Probability Density Function, Where $\alpha = 1.0$ and Various A_α

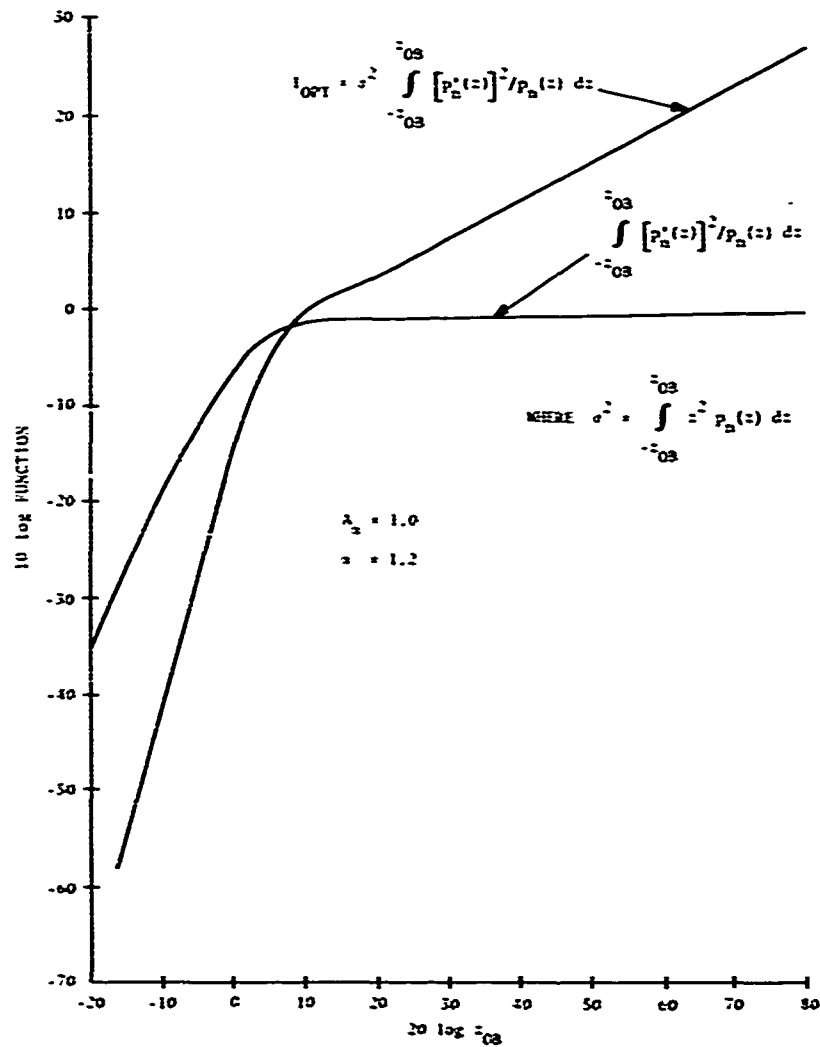


Figure 6. Variation of I_{opt} and $I_{opt} \sigma^2$ With Dynamic Range

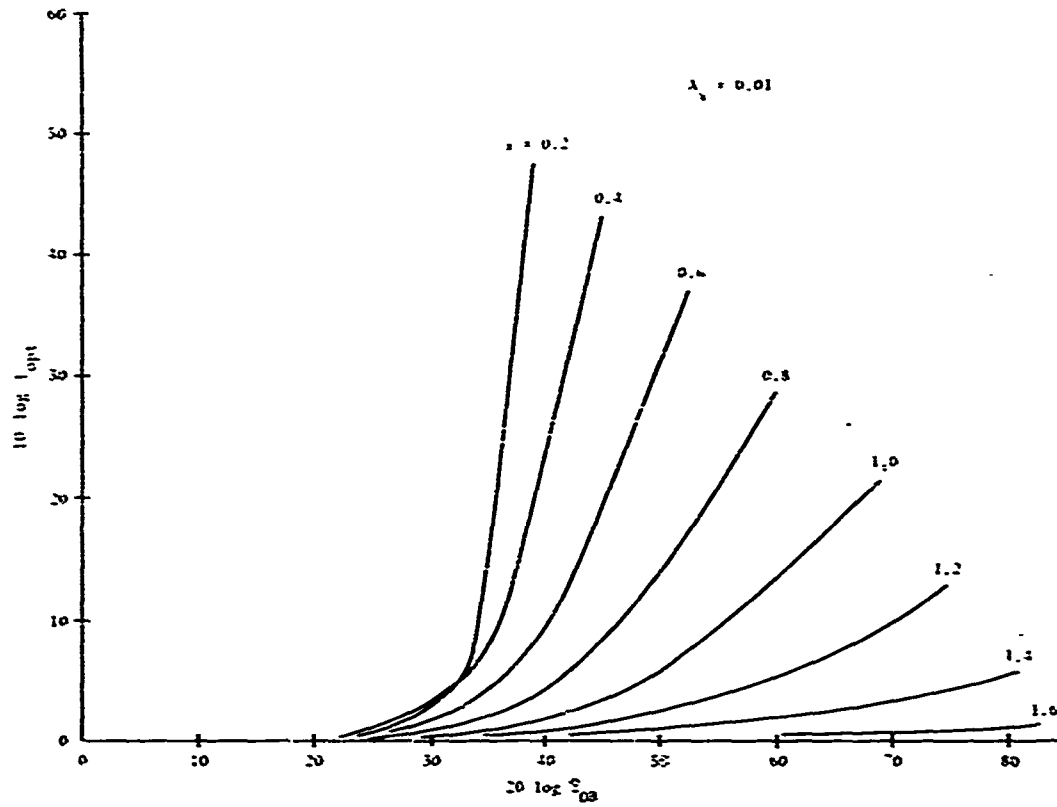


Figure 7. Improvement Factor for Optimum Nonlinearity, Where $A_\alpha = 0.01$

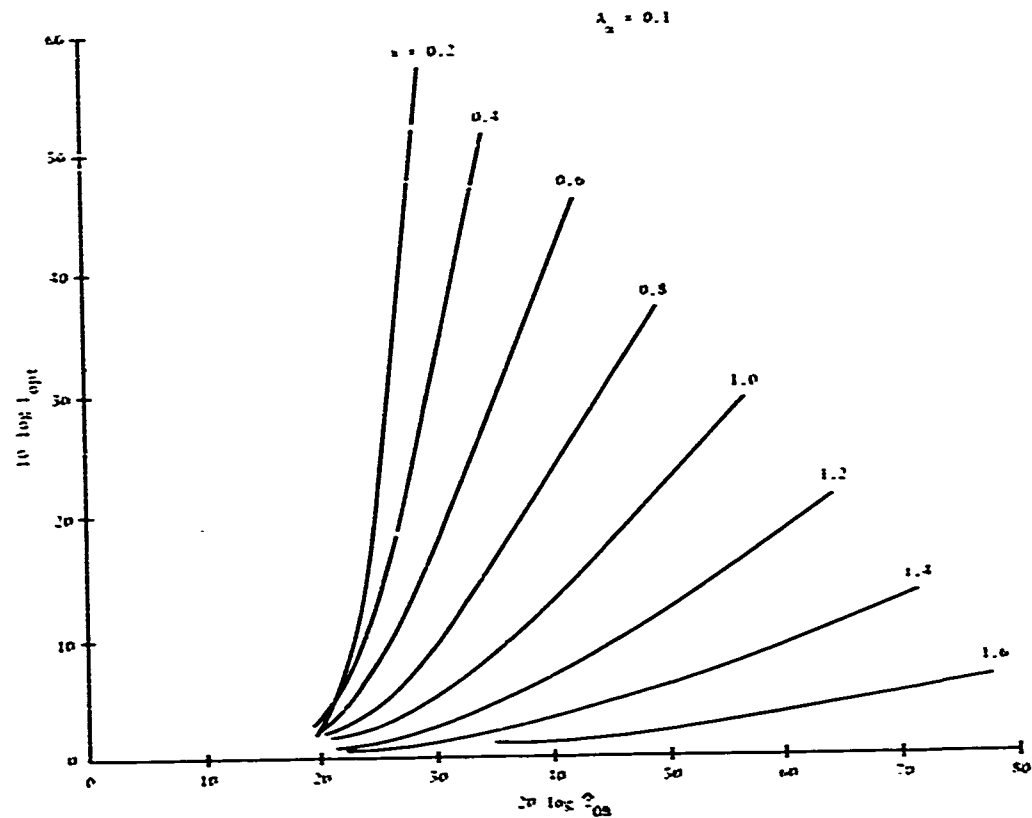


Figure 8. Improvement Factor for Optimum Nonlinearity, Where $A_\alpha = 0.1$

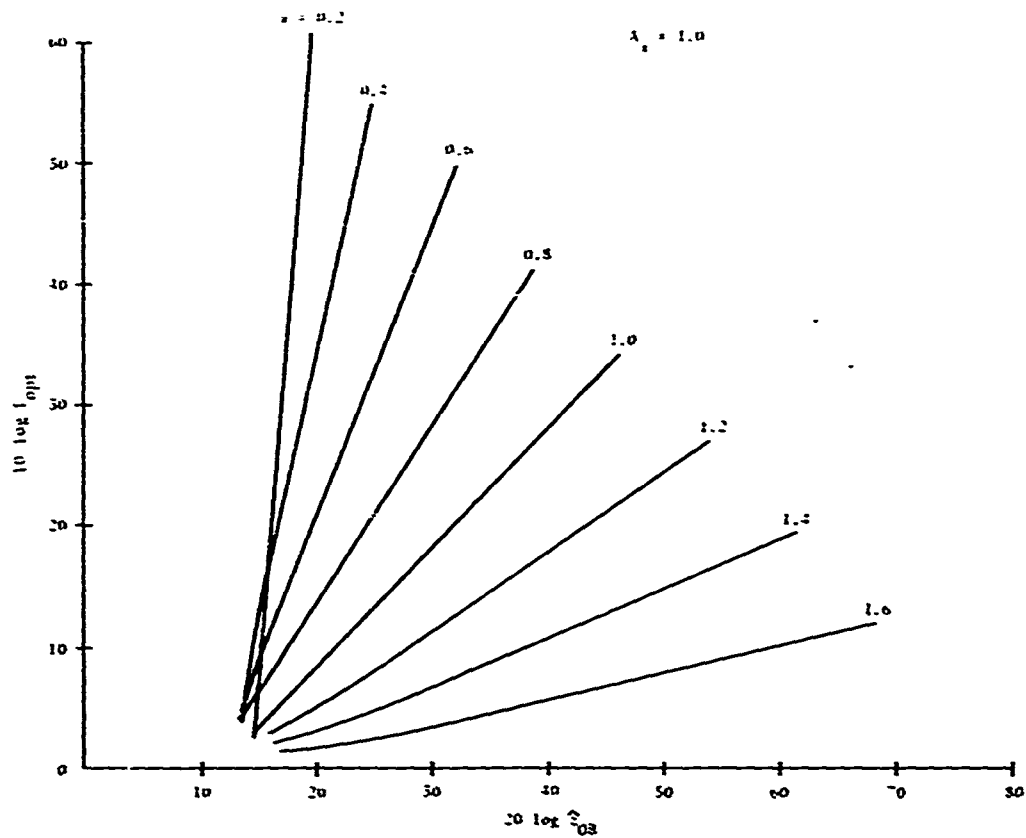


Figure 9. Improvement Factor for Optimum Nonlinearity, Where $A_\alpha = 1.0$

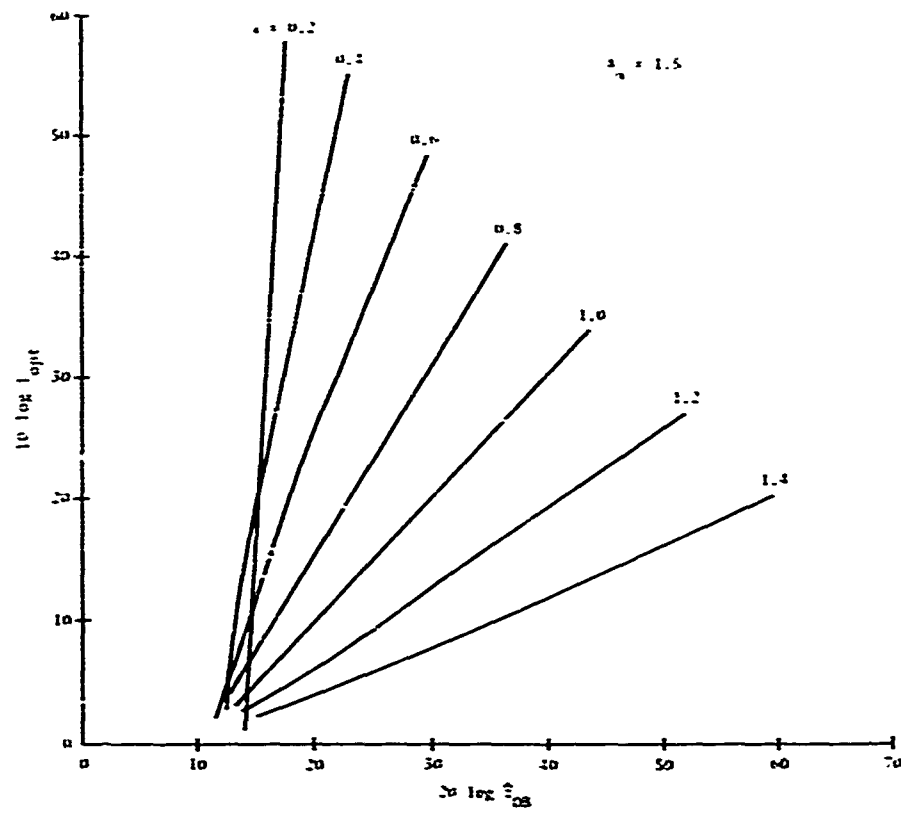


Figure 10. Improvement Factor for Optimum Nonlinearity, Where $A_\alpha = 1.5$

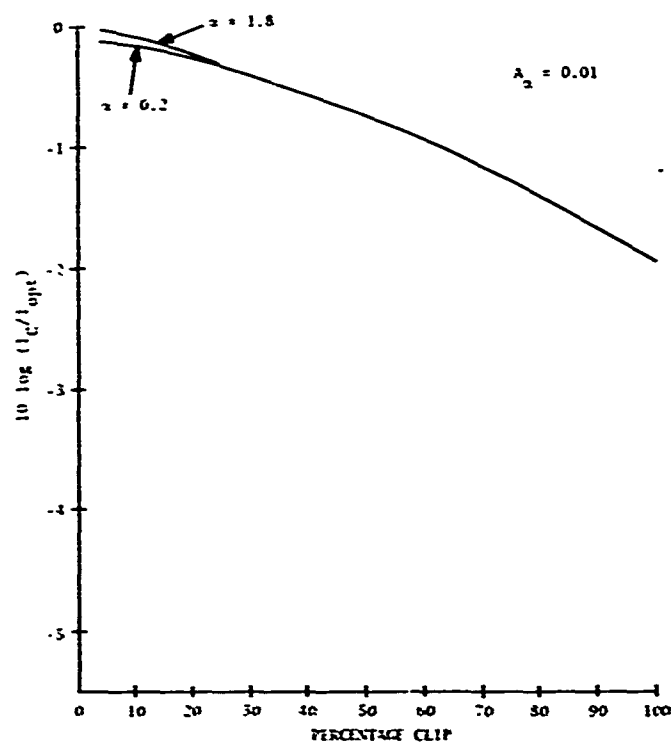


Figure 11. Clipper Performance Relative to Optimum Performance,
Where $A_\alpha = 0.01$

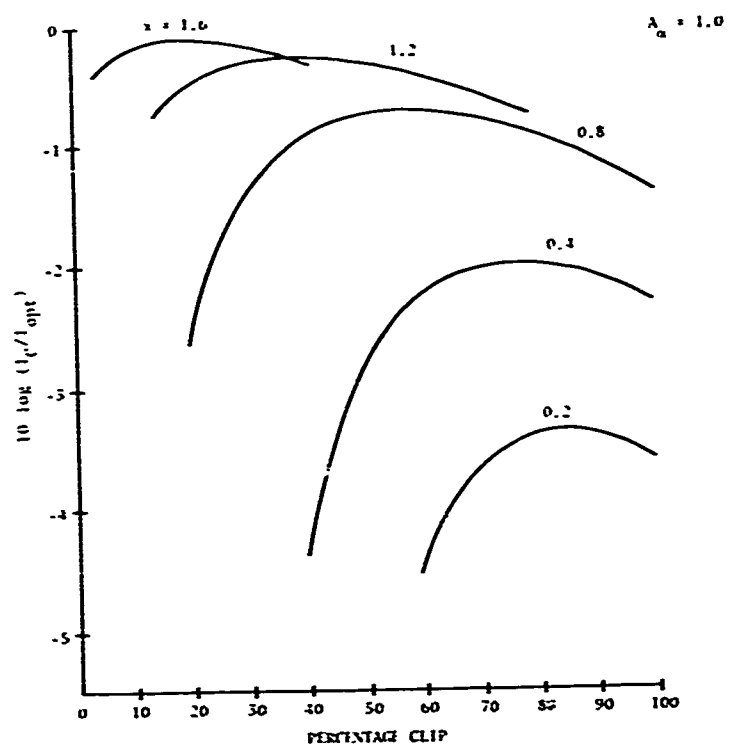


Figure 12. Clipper Performance Relative to Optimum Performance,
Where $A_{\alpha} = 1.0$

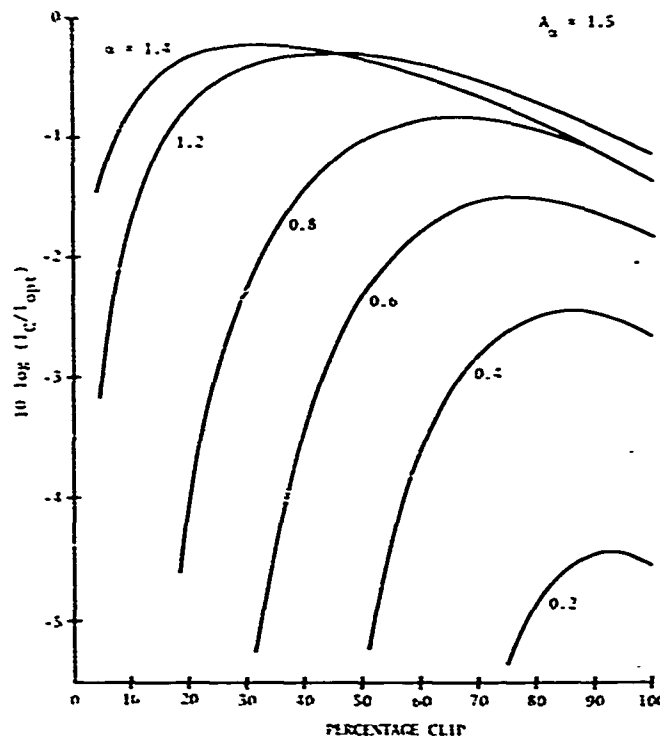


Figure 13. Clipper Performance Relative to Optimum Performance,
Where $A_\alpha = 1.5$

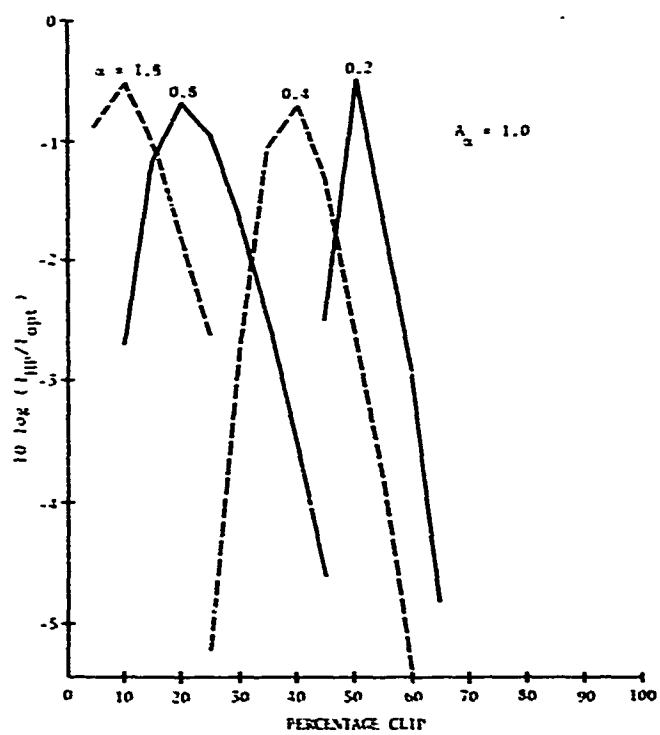


Figure 14. Hole Puncher Performance Relative to Optimum Receiver

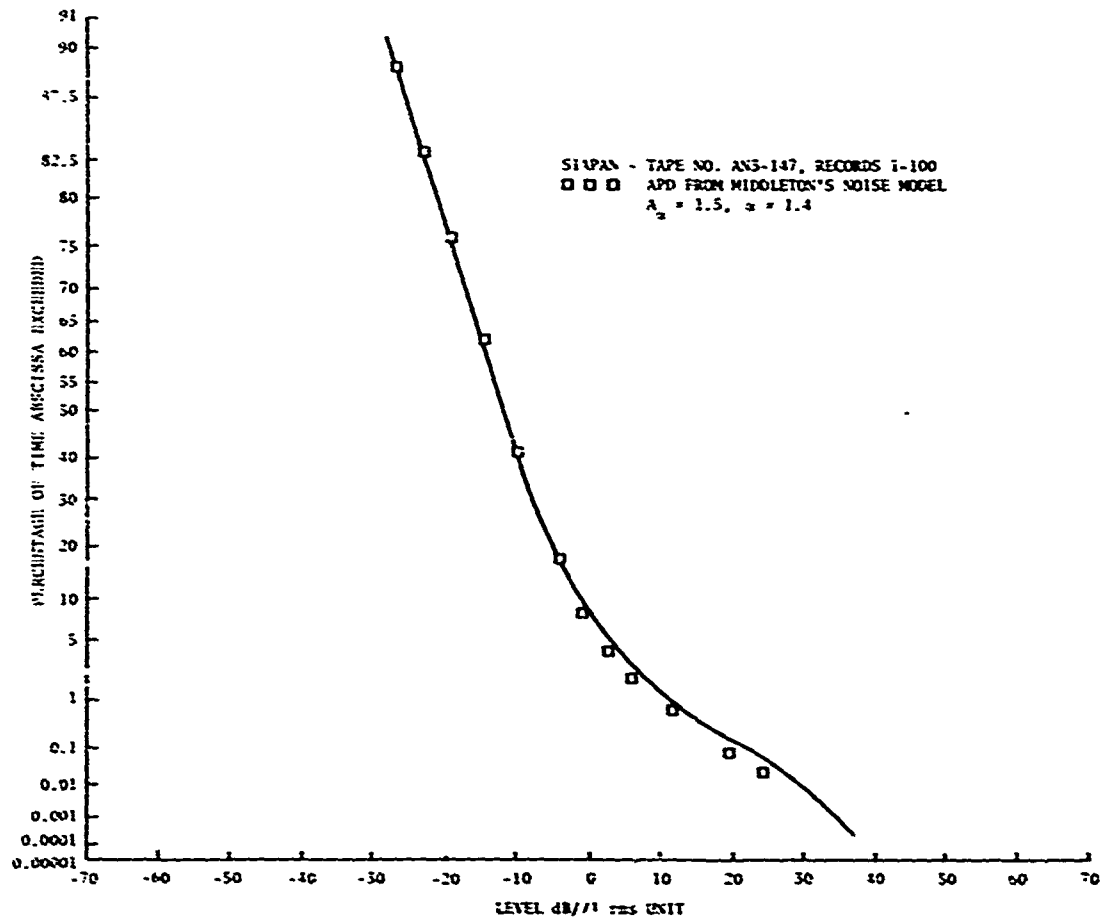


Figure 15. APD of High Level ELF Noise, Where $A_\alpha = 1.5$ and $\alpha = 1.4$

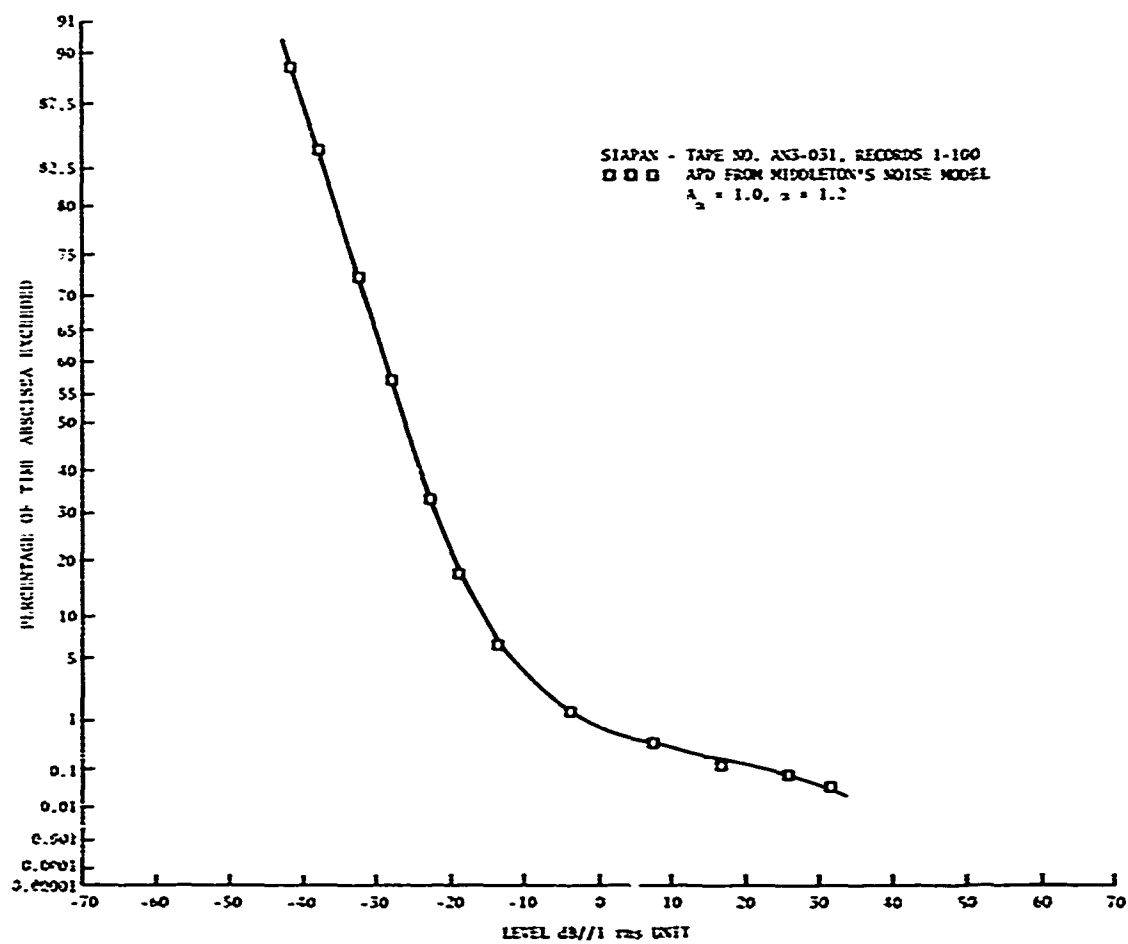


Figure 16. APD of High Level ELF Noise, Where $A_\alpha = 1.0$ and $\alpha = 1.2$

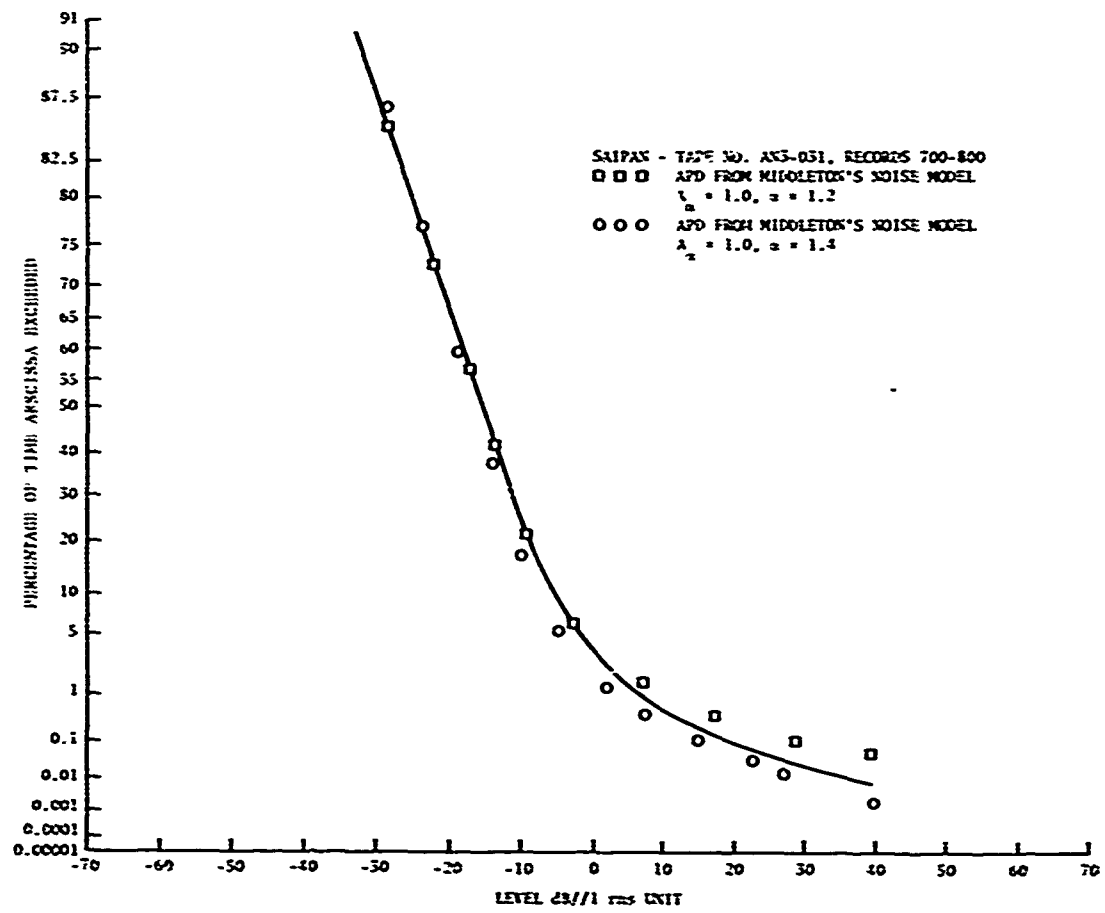


Figure 17. APD of High Level ELF Noise, Where $\lambda_n = 1.0$ and $\alpha = 1.2 - 1.4$

REFERENCES

1. J. E. Evans and A. S. Griffiths, "Design of a Sanguine Noise Processor Based on World-Wide Extremely Low Frequency (ELF) Recordings," IEEE Transactions on Communications, vol. COM-22, April 1974, pp. 528-539.
2. S. S. Rappaport and L. Kurz, "An Optimal Nonlinear Detector for Digital Data Transmission Through Non-Gaussian Channels," IEEE Transactions in Communications Technology, vol. COM-14, June 1966, pp. 266-274.
3. O. Antonov, "Optimal Detection of Signals in Non-Gaussian Noise," Radio Engineering and Electronic Physics (USSR), vol. 12, 1967, pp. 541-548.
4. A. D. Watt and E. L. Maxwell, "Measured Statistical Characteristics of VLF Atmospheric Radio Noise," Proceedings of the Institute of Radio Engineers, Inc., vol. 45, no. 1, January 1957, pp. 55-62.
5. W. Q. Crichlow, C. J. Roubique, A. D. Spaulding, and W. M. Berry, "Determination of the Amplitude Probability Distribution of Atmospheric Radio Noise from Statistical Moments," Journal of Research of the National Bureau of Standards, vol. 64 D, no. 1, January 1960, pp. 49-56.
6. H. Yuhada, T. Ishida, and M. Higashimara, "Measurement of the Amplitude Probability Distribution of Atmospheric Noise," Journal of the Radio Research Laboratory, Japan, vol. 3, no. 11, January 1956, pp. 101-109.
7. D. Middleton, Statistical-Physical Models of Man-Made Radio-Noise, Part I: First-Order Probability Models of the Instantaneous Amplitude, Office of Telecommunications, Technical Report OT-74-36, U.S. Government Printing Office, Washington, DC 20402, April 1974.
8. D. Middleton, Statistical Physical Models of Man-Made and Natural Radio Noise, Part II: First-Order Probability Models of the Envelope and Phase, Office of Telecommunications Technical Report OT-76-86, U.S. Government Printing Office, Washington, DC 20402, April 1976.
9. D. Middleton, Statistical-Physical Models of Man-Made and Natural Radio Noise, Part III: First-Order Probability Models of the Instantaneous Amplitude of Class B Interference, Office of Telecommunications Technical Report NTIA-CR-78-1, U.S. Government Printing Office, Washington, DC 20402, June 1978.
10. A. Griffiths, ELF Noise Processing, Lincoln Laboratory Technical Report 490, Massachusetts Institute of Technology, Lexington, January 1972 (DDC AD-739907).

Appendix A

DERIVATION OF THE IMPROVEMENT FACTORS
FOR SEVERAL NONLINEARITIES

In this appendix the improvement factors for the optimum nonlinearity, the hard limiter, the clipper, and the hole puncher are derived. The improvement factor is defined as the signal to noise ratio (SNR) at the correlator output, with the appropriate nonlinearity in the signal path, divided by the SNR with the nonlinearity removed. The improvement factor is an indication of the performance improvement or degradation that is expected owing to inclusion of the nonlinear device in the signal path. The test statistic at the correlator output is the sum of independent, finite variance random variables; and by the Central Limit Theorem it is asymptotically Gaussian distributed. Hence, the output SNR is sufficient for describing receiver performance for large N .

The receiver structure of interest is shown in figure A-1. Each input sample, x_i , is the sum of a completely known signal sample, S_i , and an independent noise sample, n_i . The signal samples are considered to have come from one of two binary equal-energy signals; the noise samples are identically distributed zero mean with variance σ_n^2 and have a symmetric first order amplitude probability density function. The y_i are the outputs of a zero memory nonlinearity, $f(x_i)$. The test statistic, δ , is the sum over i of N products of the form $S_i y_i$. The SNR at the correlator output is defined as the ratio of the square of the expected value of δ and the variance of δ . Remembering that the S_i are completely known, the SNR at the correlator output with the nonlinearity in the circuit is easily found to be given by

$$\text{SNR}_{NL} = \frac{\left(\sum_{i=1}^N S_i \bar{y}_i \right)^2}{\sum_{i=1}^N S_i^2 \text{Var}(y_i)} \quad (\text{A-1})$$

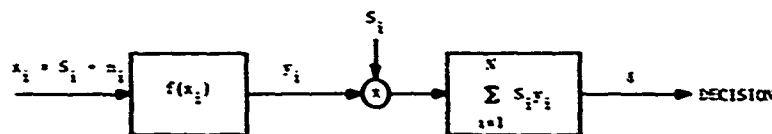


Figure A-1. Optimum Receiver Structure for Threshold Detection

With the nonlinearity removed, the SNR at the correlator output is given by

$$\text{SNR}_L = \frac{\sum_{i=1}^N S_i^2}{\sigma_n^2} \quad (\text{A-2})$$

resulting in an improvement factor, I, of

$$I = \frac{\text{SNR}_{NL}}{\text{SNR}_L} = \frac{\sigma_n^2 \left(\sum_{i=1}^N S_i \bar{y}_i \right)^2}{\left(\sum_{i=1}^N S_i^2 \right) \left(\sum_{i=1}^N S_i^2 \text{Var}(y_i) \right)} \quad (\text{A-3})$$

In order to evaluate the improvement factor for the various nonlinearities of interest, the mean and variance of the samples at the nonlinear output are needed.

For threshold signals in independent, identically distributed noise, the optimum nonlinearity takes the form

$$y_i = f(x_i) = - \frac{d}{dx_i} \ln p_n(x_i) \quad (\text{A-4})$$

where $p_n(x_i)$ is the amplitude probability density function of the noise-only samples. The expected value of y_i is given by

$$\bar{y}_i = \int_{-\infty}^{\infty} \left[- \frac{d}{dx_i} \ln p_n(x_i) \right] p_n(x_i - S_i) dx_i \quad (\text{A-5})$$

It is possible to expand $p_n(x_i - S_i)$ in a Taylor series about x_i , and the terms in S_i of order two and greater can be dropped for threshold signals. Then, using the fact that $p_n(x_i)$ is symmetrical, \bar{y}_i is found to be

$$\bar{y}_i = S_i L \quad (\text{A-6})$$

$$L = \int_{-\infty}^{\infty} \frac{[p_n'(x_i)]^2}{p_n(x_i)} dx_i \quad .$$

Using a similar approach, we find the variance of the nonlinear output to be

$$\text{Var}(y_i) = L(1 - S_i^2 L) \quad (\text{A-7})$$

The improvement factor for the optimum nonlinearity is, then, given by

$$I_{\text{opt}} \geq \frac{\sigma_n^2}{\text{SNR}_L} \int_{-\infty}^{\infty} \frac{[p_n'(x_i)]^2}{p_n(x_i)} dx_i \quad (\text{A-8})$$

with equality as $S_i^2 L$ approaches zero.

The hard limiter is defined by a transfer function such that $y_i = +1$ $x_i \geq 0$ and $y_i = -1$ for $x_i < 0$. The expected value of y_i is given by

$$\bar{y}_i = 2 \left[\int_0^{\infty} p_n(x_i - S_i) dx_i \right] - 1, \quad (\text{A-9})$$

where the expression within the brackets is simply the probability of $y_i = +1$. Since we are interested in comparing the various nonlinearities under similar signal conditions, i.e., threshold signals, S_i can be assumed small. For small S_i and a symmetrical noise density function,

$$\bar{y}_i = 2S_i p_n(0) \quad (\text{A-10})$$

and

$$\text{Var}(y_i) = 1 - 4S_i^2 p_n^2(0) \quad (\text{A-11})$$

Substituting equations (A-10) and (A-11) into (A-3) yields the improvement for the hard limiter,

$$L_{HL} \geq 4\sigma_n^2 p_n^2(0) \quad (\text{A-12})$$

with equality as $4S_i^2 p_n^2(0)$ approaches zero.

The clipper is described by a transfer function such that

$$y_i = \begin{cases} x_i & -c \leq x_i \leq c \\ +c & x_i > c \\ -c & x_i < -c, \end{cases} \quad (\text{A-13})$$

where c is a constant greater than zero. The expected value of y_i is found from

$$\bar{y}_i = \int_{-c}^c x_i p_n(x_i - S_i) dx_i + \int_c^{\infty} c p_n(x_i - S_i) dx_i + \int_{-\infty}^{-c} (-c) p_n(x_i - S_i) dx_i. \quad (\text{A-14})$$

Again, letting S_i become small,

$$\bar{y}_i = S_i p,$$

where

$$p = 2 \int_0^c p_n(x_i) dx_i. \quad (\text{A-15})$$

in a similar manner, the variance of the clipper output can be found:

$$\text{Var}(y_i) = 2 \int_0^c x_i^2 p_n(x_i) dx_i + c^2(1 - p). \quad (\text{A-16})$$

Substituting the above expressions into (A-3) yields the improvement factor for the clipper:

$$I_C = \frac{\sigma_n^2 p^2}{2 \int_0^c x_i^2 p_n(x_i) dx_i + c^2(1 - p)}. \quad (\text{A-17})$$

The hole puncher is similar to the clipper except that the output is set to zero if the input exceeds the threshold c . The mean and variance at the output of the hole puncher are found by following the procedure utilized with the clipper. The mean is given by

$$\bar{y}_i = S_i [p - 2c p_n(c)], \quad (\text{A-18})$$

where p was defined in equation (A-15) and $p_n(c)$ is the noise density function evaluated at c . The variance is given by

$$\text{Var}(y_i) = 2 \int_0^c x_i^2 p_n(x_i) dx_i \quad (\text{A-19})$$

and the improvement factor by

$$I_{HP} = \frac{\sigma_n^2 [p - 2c p_n(c)]^2}{2 \int_0^c x_i^2 p_n(x_i) dx_i}. \quad (\text{A-20})$$

It is interesting to note that while the SNR's at the correlator output depend on the signal structure, the improvement factors for the four nonlinearities of interest are independent of the values of the signal samples. This is a result of the small SNR assumption.

Appendix B

NUMERICAL COMPUTATION OF THE
HYPERGEOMETRIC AND GAMMA FUNCTIONS

Inherent within the results of this report is the need to evaluate the density function, $p_n(z)$, for Middleton's Class B Noise Model and its derivative, $p'_n(z)$. These functions are expressed in equations (B-1) and (B-2); $p'_n(z)$ is derived from $p_n(z)$ with the aid of the following identities:

$$\frac{d}{dz} {}_1F_1(a; b; z) = \frac{a}{b} {}_1F_1(a + 1; b + 1; z)$$

$$a\Gamma(a) = \Gamma(a + 1)$$

$$p_n(z) \cong p_I(z) = \frac{1}{\pi} \sum_{m=0}^{\infty} \frac{(-1)^m A_{\alpha}^m}{m!} \Gamma\left(\frac{m\alpha + 1}{2}\right) {}_1F_1\left(\frac{m\alpha + 1}{2}; \frac{1}{2}; -z^2\right) \quad |z| \leq z_{OB} \quad (\text{B-1})$$

$$p'_n(z) = \frac{d}{dz} p_n(z) = \frac{-4z}{\pi} \sum_{m=0}^{\infty} \frac{(-1)^m A_{\alpha}^m}{m!} \Gamma\left(\frac{m\alpha + 3}{2}\right) {}_1F_1\left(\frac{m\alpha + 3}{2}; \frac{3}{2}; -z^2\right) \quad |z| \leq z_{OB}' \quad (\text{B-2})$$

where

$$0 < \alpha < 2 \quad A_{\alpha} > 0$$

$\Gamma(a)$ = Gamma Function

${}_1F_1(a; b; c)$ = Confluent Hypergeometric Function.

Thus, both $p_n(z)$ and its derivative require computing the Hypergeometric Function, ${}_1F_1(a; b; -z)$, and the Gamma Function, $\Gamma(a)$. For all values of α and the index of summation, m , indicated in equations (B-1) and (B-2), the parameters a , b , and z satisfy $a \geq b > 0$, and $z \geq 0$. This appendix outlines the algorithms used in this report to compute the Hypergeometric and Gamma Functions for these ranges of arguments.

The Confluent Hypergeometric Function, ${}_1F_1(a; b; -z)$, is defined in equation (B-3). This equation, however, is suitable for the numerical computation of ${}_1F_1(a; b; -z)$ only for small arguments of a and z . Thus, equations (B-4) through (B-6) are needed to evaluate the Hypergeometric Function for a broader range of arguments, in particular large z :

$${}_1F_1(a; b; -z) = \sum_{i=0}^{\infty} \frac{(a)_i (-1)^i z^i}{(b)_i i!} \quad (B-3)$$

$${}_1F_1(a; b; -z) = e^{-z} {}_1F_1(b-a; b; z) \quad (B-4)$$

$$(b-a) {}_1F_1(a-1; b; -z) + (2a-b-z) {}_1F_1(a; b; -z) - a {}_1F_1(a+1; b; -z) = 0 \quad (B-5)$$

$${}_1F_1(a; b; -z) \cong \frac{\Gamma(b)}{\Gamma(b-a)} z^{-a} \sum_{i=0}^N \frac{(a)_i (a+1-b)_i}{i! z^i} \quad (z \gg 0), \quad (B-6)$$

where

$$(a)_i = a(a+1)(a+2)\cdots(a+i-1) = \prod_{j=0}^{i-1} (a+j); \quad (a)_0 \triangleq 1$$

N = index of the smallest term in equation (B-6).

Whereas equations (B-3) through (B-5) are identities, equation (B-6) is an asymptotic series approximation to the Hypergeometric Function valid only for large z with respect to a and b . Note, however, that this asymptotic series is divergent for any given z since

$$\begin{aligned} \lim_{n \rightarrow \infty} \left| \frac{t_{n+1}}{t_n} \right| &= \lim_{n \rightarrow \infty} \frac{t_{n+1}}{t_n} = \lim_{n \rightarrow \infty} \frac{\left(\frac{(a)_{n+1} (a+1-b)_{n+1}}{(n+1)! z^{n+1}} \right)}{\left(\frac{(a)_n (a+1-b)_n}{n! z^n} \right)} \\ &= \lim_{n \rightarrow \infty} \frac{(a+n) (a+1-b+n)}{(n+1) z} = \infty \end{aligned}$$

Hence, the point of truncation of the series, N , is important when using equation (B-6) to approximate the Hypergeometric Function.

To understand the behavior of the terms of this asymptotic expansion, consider the following:

$$\begin{aligned} t_{n+1} - t_n &= \frac{(a)_{n+1} (a+1-b)_{n+1}}{(n+1)! z^{n+1}} - \frac{(a)_n (a+1-b)_n}{n! z^n} \\ &= \frac{(a)_n (a+1-b)_n}{(n+1)! z^{n+1}} \left[(a+n) (a+1-b+n) - (n+1)z \right] \end{aligned}$$

Since $(a)_n(a+1-b)_n/(n+1)! z^{n+1}$ is positive, the sign of $t_{n+1} - t_n$ is determined by the quadratic equation

$$\begin{aligned} & [(a+n)(a+1-b+n) - (n+1)z] \\ &= [n^2 + (2a+1-b-z)n + (a^2 + a - ab + z)], \end{aligned}$$

which has roots at

$$n_1, n_2 = (z + b - 2a - 1 \mp \sqrt{z^2 + 2z(1+b-2a) + (1-b)^2})/2.$$

Figure (B-1) is a graphical representation of this quadratic function.

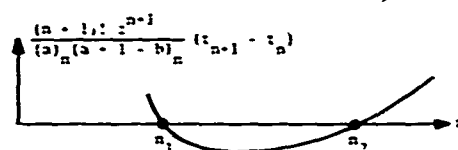


Figure B-1. Graphical Representation of the Quadratic

$$\text{Function } \frac{(n+1)! z^{n+1}}{(a)_n (a+1-b)} (t_{n+1} - t_n)$$

If n_1 and n_2 are both less than zero, equation (B-6) diverges immediately and should not be used to approximate the Hypergeometric Function for the given values of a , b , and z . If, however, n_1 and n_2 are of the opposite sign, the terms of the series initially decrease in value until $n = n_2$ and, then, grow indefinitely. When both n_1 and n_2 are positive, the terms initially increase in value, then decrease, and finally grow indefinitely again. In these latter two cases, one can find the smallest term of the series (i.e., the stopping point) by comparing the $(n+1)^{\text{th}}$ term with the n^{th} term only after the index exceeds n_1 . Thus, if $n > n_1$, $t_{n+1} > t_n$ and $t_n < t_0 = 1$ are all satisfied, the stopping index N equals n . If this last condition, $t_n < t_0$, is the only one not satisfied, the first term of the expansion, t_0 , must be the smallest and N is set equal to 0.

The computation of $p_n(z)$ or $p'_n(z)$ for a particular z requires evaluating the Hypergeometric Function via a series in which the "a" argument $[(m\alpha/2) + b]$ is a linear function of the index of summation and is, therefore, increasing as more terms are included in the series. For large z , one hopes that the asymptotic expression (equation (B-6)) can be used, and that the $A_{\alpha}^m \Gamma(\cdot)/m!$ factor in equations (B-1) and (B-2) decreases rapidly enough so that only a few terms in the summation need be evaluated to satisfactorily approximate $p_n(z)$ or $p'_n(z)$. By choosing to use equation (B-6) only when $z > 10$, one can guarantee that the asymptotic expression will be valid to approximate ${}_1F_1(a; b; -z)$, for $m = 0, 1, 2$, $a = (m\alpha/2) + b$, $b = 1/2$ or $3/2$, and $0 < \alpha < 2$. If, however, the $A_{\alpha}^m \Gamma(\cdot)/m!$ factor is not decreasing rapidly enough to limit the number of terms required in equation (B-1) or (B-2), so that $a = [(m\alpha/2) + b]$ becomes too large to use equation (B-6) to approximate the Hypergeometric Function for the given z , then equation (B-6) may be used on $a - 1$ or $a - 2 \dots$, and then equation (B-5) can be utilized to iterate on "a" back to its original value.

This iteration technique was also used to evaluate the Gamma Function, $\Gamma(z)$, which appears with positive arguments in equations (B-1) and (B-2) and negative arguments in equation (B-6). A polynomial approximation to $\Gamma(z)$ (equation (B-7)) was used on the fractional part of the argument, thereby requiring one to use the recursion relationship in equation (B-8) to step the argument up or down to its desired value:

$$\Gamma(z + 1) \cong 1 + \sum_{i=1}^8 c_i z^i \quad 0 \leq z \leq 1 \quad (\text{B-7})$$

$$z\Gamma(z) = \Gamma(z + 1) \quad (\text{B-8})$$

$$\Gamma(z) \cong e^{-z} z^{(z-\frac{1}{2})} \sqrt{2\pi} e^{(1/12z)} \quad 30 \leq z \leq 55, \quad (\text{B-9})$$

where

$c_1 = -0.577191652$	$c_5 = -0.756704078$
$c_2 = 0.988205891$	$c_6 = 0.482199$
$c_3 = -0.897056937$	$c_7 = -0.193527818$
$c_4 = 0.918206857$	$c_8 = 0.035868343$

Figures B-2 and B-3 are flow diagrams of the algorithms used in this report to evaluate the Hypergeometric and the Gamma Functions, respectively.

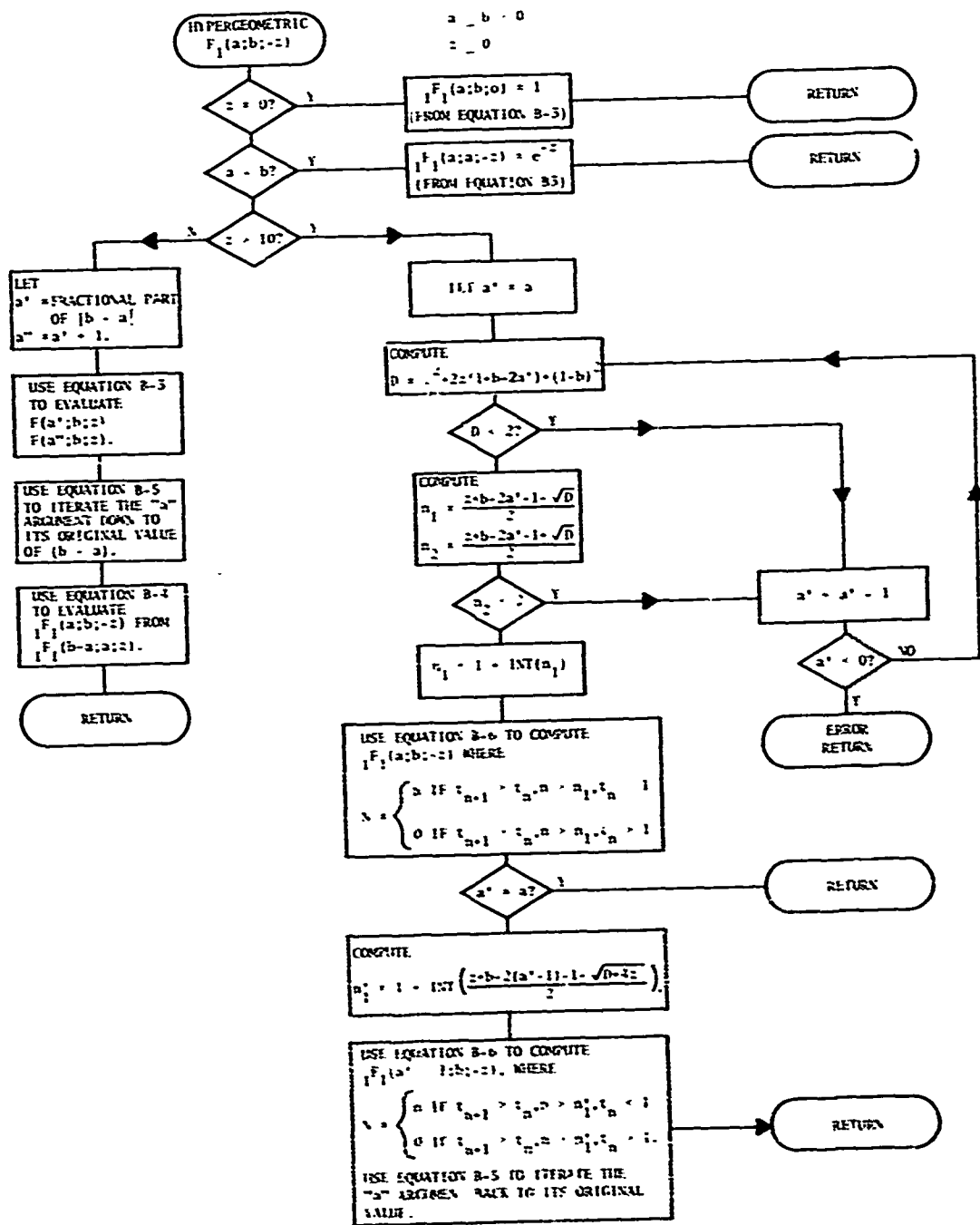


Figure B-2. Flow Diagram for Evaluating the Hypergeometric Function

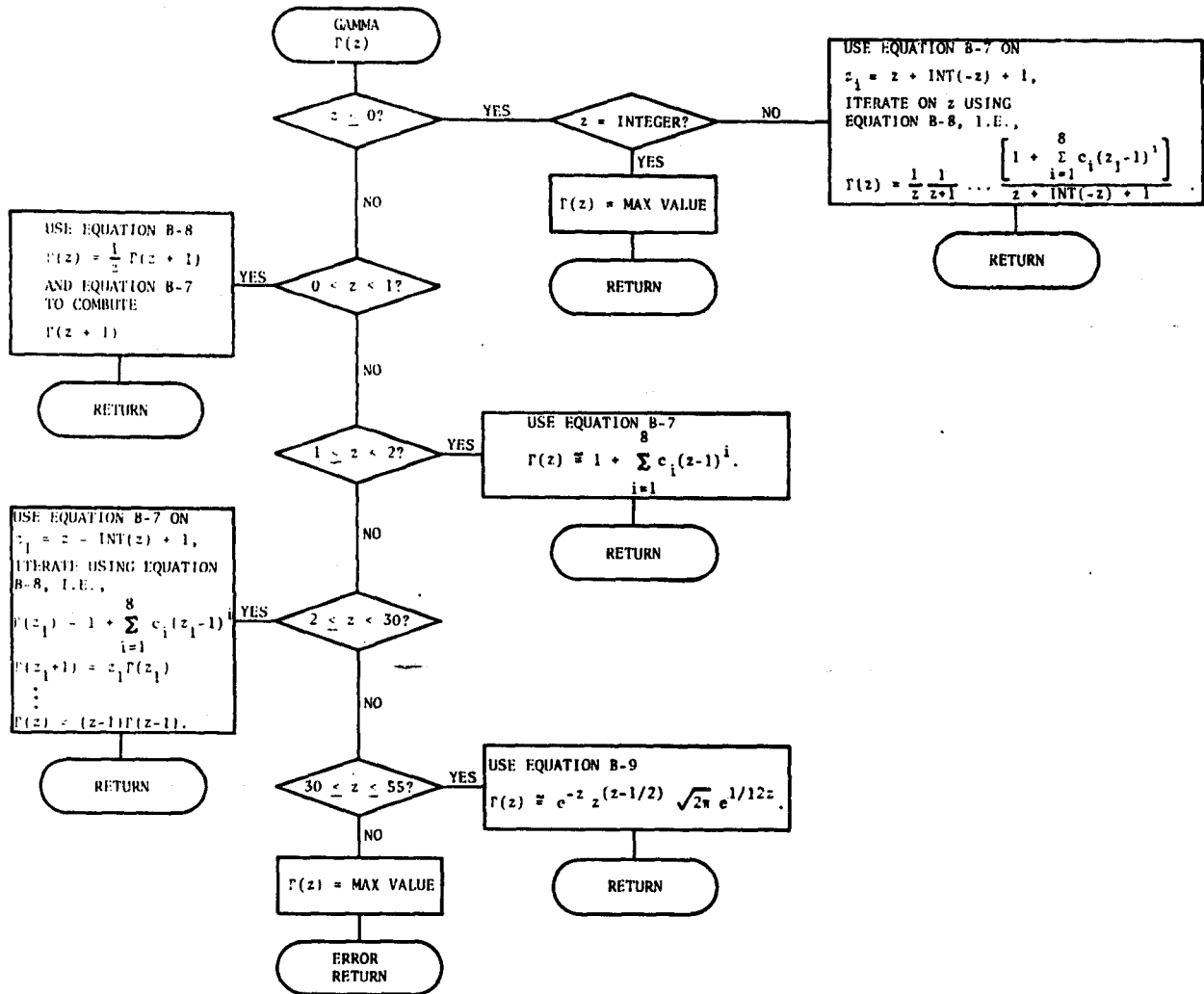


Figure B-3. Flow Diagram for Evaluating the Gamma Function

INITIAL DISTRIBUTION LIST

ADDRESSEE	No. of Copies
OUSDRGE (Research & Advanced Technology)(W. J. Perry)	2
CNO, OP-098, -941	2
CNM, MAT-08T1 (CAPT S. F. Parrish)	1
NRL, 7500 (J. Davis)	1
NORDA (R. Goodman, 110)	1
NAVOCEANO	1
COMNAVSECGRU, G83 (D. Clark)	1
NAVELECSYSCOM, ELEX 310 (M. Parker), PME-107 (Lawson), -108, -117 (LeFaude, Kruger, Brunkart)	6
NAVSEASYSCOM, SEA-611 (Coscarelli)	1
NAVAIRDEVCEN	1
NAVAIRDEVCEN, Code 2052	1
NOSC, Code 810	1
NOSC, Code 6565	1
DTNSRDC	1
NAVSURFWPNCEN	1
CHESNAVFACENCOM, FPO-1P3	1
NAVPGSCOL	1
NAVTRAEQUIPCENT, Technical Library	1
APL/UW, SEATTLE	1
ARL/PENN STATE, STATE COLLEGE	1
IBM, Burlington, VT (R. Houle)	1
PURVIS Systems Inc., San Diego, CA (A. Morrison)	1
Sperry Research Ctr., 100 North Rd., Sudbury, MA (J. Toomey)	1
GTE Sylvania Inc., 189B Street, Needham Heights, MA (F. Casselman)	1
Asst. Secty Defense, C3I (T. Quinn)	1
National Telecommunications and Information Administration, Institute for Telecommunication Sciences, Boulder, Colo. (A. D. Spaulding)	1
DTIC	12